Wavelets linked by differentiation-integration on the unit interval and related applications

Souleymane Kadri Harouna, Valérie Perrier

Numerical Algorithms manuscript No.
(will be inserted by the editor)

Wavelets linked by differentiation-integration on the unit interval and related applications

Kadri Harouna Souleymane · Perrier Valérie

Received: date / Accepted: date

Abstract This paper presents a new construction of biorthogonal multiresolution analyses of $L^2(0,1)$ linked by differentiation and integration. The arising wavelets basis is setted to satisfy homogeneous Dirichlet boundary condition, while this requirement is not necessary for the scaling function basis. On this wavelet basis, the solution of Poisson equation is computed by a wavelet coefficients renormalization like in Fourier domain with a linear complexity $\mathcal{O}(N)$. Fast algorithms are provided and illustrated by numerical examples.

Keywords wavelet on the interval · boundary condition · Poisson equations

1 Introduction

Since the pioneering work of Lemarié-Rieusset [15], due to their important role in the construction of divergence-free or curl-free wavelets, biorthogonal multiresolution analyses linked by differentiation and integration have been widely studied [14,18,20,21]. The main purpose was to construct two multiresolution analyses of $L^2(0,1)$ provided by spaces V_j^1 and V_j^0 such that

$$\forall\ j,\quad \frac{d}{dx}V_j^1 = V_j^0. \tag{1}$$

Relation (1) should be interpreted as: $\forall f \in V_j^1$, $f' \in V_j^0$ and $\forall g \in V_j^0$, there exists $f \in V_j^1$ such that $f' = g$.

On the unit interval $[0,1]$, with non periodic boundary conditions, such a construction was introduced firstly by Jouini and Lemarié-Rieusset [14]. They started

Kadri Harouna Souleymane
Laboratoire de Mathématiques, Image et Applications, Avenue Michel Crépeau, 17042 La Rochelle cedex 1 France E-mail: souleymane.kadri_harouna@univ-lr.fr

Perrier Valérie
Laboratoire Jean Kuntzmann, Université de Grenoble et CNRS, BP 53, 38401 Grenoble cedex 9 France E-mail: valerie.perrier@imag.fr

with V_j^1 as a *regular* multiresolution analysis reproducing polynomial at boundaries [1,5,12], with the scaling function φ^1 and wavelet ψ^1 generators that satisfy [15]:

$$(\varphi^1)'(x) = \varphi^0(x) - \varphi^0(x-1) \quad \text{and} \quad (\psi^1)' = 4\psi^0. \tag{2}$$

Jouini and Lemarié-Rieusset [14] used the orthogonal construction of [5] for the space V_j^1. They show that, from relation (2) and properly setting the integers parameters in the construction of V_j^1, one can deduce the space V_j^0 that satisfies (1). In this case, the wavelet space W_j^0 is defined by differentiating the wavelet basis of W_j^1:

$$W_j^0 = span\{\psi_{j,k}^0 := 2^{-j}(\psi_{j,k}^1)'\}.$$

The corresponding biorthogonal spaces $(\tilde{V}_j^1, \tilde{V}_j^0)$ are respectively constructed again using integration by part [6]. However, the construction of [14] remains theoretical, for instance it is not easy to compute numerically the wavelet filter of $\psi_{j,k}^0$ and $\tilde{\psi}_{j,k}^0$:

$$\psi_{j,k}^0 = \sum_n H_{k,n}^0 \varphi_{j+1,n}^0 \quad \text{and} \quad \tilde{\psi}_{j,k}^0 = \sum_n \tilde{H}_{k,n}^0 \tilde{\varphi}_{j+1,n}^0. \tag{3}$$

This point was relieved by Kadri-Harouna and Perrier [18], they extend the construction of [14] to any *regular* scaling function generator φ^1 and provided numerical algorithm and examples for the fast wavelet transform.

One advantage of the construction [14,18] is that the associated multiscale projectors commute with differentiation in $H^1(0,1)$ and these properties enable to demonstrate the Ladysenskaya-Babuska-Brezzi (LBB) condition for a wavelet based method in the numerical discretization of mixed problem such as Stokes problem [3,7]. The key ingredient is that, commutation with derivation allows to get easily the condition of Fortin's lemma [11], see [7].

Ensuring the commutation of multiscale projectors with differentiation imposes to the biorthogonal space $\tilde{V}_j^0$ to satisfy homogeneous Dirichlet boundary condition. In this case, $\tilde{V}_j^0 \subset H_0^1(0,1)$ cannot be a multiresolution analysis of $L^2(0,1)$. Moreover, relation (2) remains valid only for internal scaling functions and wavelets. Nonetheless, the edge functions did not satisfy this relation: a change of basis is introduced [19].

Recently, Stevenson [20] has proposed another construction which differs from the existing constructions by the choice of the boundaries conditions for the dual spaces $\tilde{V}_j^0$ and $\tilde{V}_j^1$. Precisely, let us suppose that $\psi_{j,k}^1$ and $\tilde{\psi}_{j,k}^0$ are the wavelets constructed from scaling function generators satisfying (2). Then, integration by part shows that:

$$\psi_{j,k}^1(1)\tilde{\psi}_{j,k}^0(1) - \psi_{j,k}^1(0)\tilde{\psi}_{j,k}^0(0) = \langle \psi_{j,k}^0, \tilde{\psi}_{j,k}^0 \rangle - \langle \psi_{j,k}^1, \tilde{\psi}_{j,k}^1 \rangle. \tag{4}$$

If the two systems $(\psi_{j,k}^1, \tilde{\psi}_{j,k}^1)$ and $(\psi_{j,k}^0, \tilde{\psi}_{j,k}^0)$ are biorthogonal, the boundaries terms of (4) should vanish. Instead of taking $\tilde{\psi}_{j,k}^0 \in H_0^1(0,1)$ like in [14], the construction of [20] sets $\psi_{j,k}^1(1) = 0$ and $\tilde{\psi}_{j,k}^0(0) = 0$. This choice of boundary condition is more general and leads to $\tilde{V}_j^0$ as a multiresolution analysis of $L^2(0,1)$, however the commutation of multiscale projector with differentiation is lost.

The focal point of his work is the construction of wavelet bases for biorthogonal multiresolution analyses of $L^2(0,1)$ linked by differentiation and integration [14, 18, 20]. As for the internal wavelets (2), emphasis is maid on the construction of edges wavelet in order to get a diagonal differentiation relation:

$$\psi^1_{j,k}(x) = 2^j \int_0^x \psi^0_{j,k}(t)dt \quad \text{and} \quad (\psi^1_{j,k})'(x) = 2^j \psi^0_{j,k}(x). \tag{5}$$

We start with the construction of wavelets $\psi^0_{j,k}$ and $\tilde{\psi}^0_{j,k}$: for this step, we will use a classical biorthogonal or orthogonal wavelet bases on the interval $[0,1]$. Since $\int_0^1 \psi^0_{j,k}(t)dt = 0$, relation (5) leads to $\psi^1_{j,k} \in H^1_0(0,1)$ instead of $\psi^1_{j,k} \in H^1(0,1)$ and $\tilde{\psi}^0_{j,k} \in H^1_0(0,1)$ as in [14, 18, 20, 21]. Moreover, from the multiscale decomposition

$$V^1_j = V^1_{j_{min}} \oplus W^1_{j_{min}} \oplus \cdots \oplus W^1_{j-1}, \tag{6}$$

we see that incorporating homogeneous Dirichlet boundary condition in V^1_j is reduced to the treatment of this boundary condition only at the coarse scale j_{min}. Taking $\psi^0_{j,k} = \tilde{\psi}^0_{j,k}$, which is the orthogonal setting, gives:

$$< (\psi^1_{j,k})', (\psi^1_{\ell,n})' >= 2^{j+\ell} < \psi^0_{j,k}, \psi^0_{\ell,n} >= 2^{j+\ell} \delta_{j,\ell} \delta_{k,n}. \tag{7}$$

Then, from (7) we infer that 1D Poisson equation with homogeneous Dirichlet boundary can be solved with a linear numerical complexity in the multiresolution analysis provided by spaces V^1_j. Furthermore, this new construction still maintains the properties of Fortin's lemma [11] in the numerical discretization of Stokes problem and allows to get a fast divergence-free wavelet transform algorithm similar to the periodic case [10]. The main difficulties of such a construction is the numerical implementation of the decomposition (6), this point will be well documented in the present work.

In Section 2 we recall the construction of biorthogonal multiresolution analysis of $L^2(0,1)$ with polynomial reproduction and how to impose homogeneous boundary conditions. Section 3 reminds the principle of the construction of BMRA linked by differentiation / integration and its main properties needed for a numerical implementation. The new construction of BMRA linked by differentiation / integration is detailed in Section 4 where the associated fast wavelet transform algorithms are provided.

2 Biorthogonal multiresolution analyses of $L^2(0,1)$ reproducing polynomial

The construction of biorthogonal multiresolution analyses $(V_j, \tilde{V}_j)$ of $L^2(0,1)$ with polynomial reproduction $(r, \tilde{r})$ is classical [4, 8, 12]: the principle is to start with generators $(\varphi, \tilde{\varphi})$, that are biorthogonal scaling functions of a BMRA on $\mathbb{R}$. We

suppose that φ is compactly supported on $[n_{min}, n_{max}]$ and reproduces polynomials up to degree $r-1$:

$$0 \leq \ell \leq r-1, \quad \frac{x^\ell}{\ell!} = \sum_{k=-\infty}^{+\infty} \tilde{p}_\ell(k)\ \varphi(x-k), \quad \forall\ x \in \mathbb{R}, \tag{8}$$

with $\tilde{p}_\ell(k) = \langle \frac{x^\ell}{\ell!}, \tilde{\varphi}(x-k) \rangle$. Similarly, $\tilde{\varphi}$ reproduces polynomials up to degree $\tilde{r}-1$ and we note $p_\ell(k) = \langle \frac{x^\ell}{\ell!}, \varphi(x-k) \rangle$. For j sufficiently large, the spaces V_j on $[0,1]$ have the structure:

$$V_j = V_j^\flat \oplus V_j^{int} \oplus V_j^\sharp, \tag{9}$$

where $V_j^{int} = span\{\varphi_{j,k}(x) = 2^{j/2}\varphi(2^j x - k)\ ;\ k = k_\flat,\ 2^j - k_\sharp\}$ is the space generated by *interior scaling functions* whose supports are included into $[\frac{\delta_\flat}{2^j}, 1 - \frac{\delta_\sharp}{2^j}] \subset [0,1]$ ($\delta_\flat,\ \delta_\sharp \in \mathbb{N}$ be two fixed parameters), and $k_\flat = \delta_\flat - n_{min}$ and $k_\sharp = \delta_\sharp + n_{max}$. Moreover

$$V_j^\flat = span\{\Phi_{j,\ell}^\flat(x) = 2^{j/2}\Phi_\ell^\flat(2^j x)\ ;\ \ell = 0, \cdots, r-1\},$$
$$V_j^\sharp = span\{\Phi_{j,\ell}^\sharp(1-x) = 2^{j/2}\Phi_\ell^\sharp(2^j(1-x))\ ;\ \ell = 0, \cdots, r-1\},$$

are the *edge spaces*, the *edge scaling functions* at the edge 0 being defined in order to preserve the polynomial reproduction (8) on the interval $[0,1]$:

$$0 \leq \ell \leq r-1, \quad \Phi_\ell^\flat(x) = \sum_{k=1-n_{max}}^{k_\flat - 1} \tilde{p}_\ell(k)\ \varphi(x-k)\ \chi_{[0,+\infty[}. \tag{10}$$

At the edge 1, the edge scaling functions $\Phi_{j,\ell}^\sharp$ are constructed on $]-\infty, 1]$ by symmetry, using the transform $Tf(x) = f(1-x)$. In practice we have to choose $j \geq j_{min}$ where j_{min} is the smallest integer which verifies $j_{min} > \log_2[n_{max} - n_{min} + \delta_\sharp + \delta_\flat]$ to ensure that the supports of edge scaling functions at 0 do not intersect the supports of edge scaling functions at 1.

The polynomial reproduction in V_j is then satisfied since, for $0 \leq \ell \leq r-1$ and $x \in [0,1]$ we have:

$$\frac{2^{j/2}(2^j x)^\ell}{\ell!} = 2^{j/2}\Phi_\ell^\flat(2^j x) + \sum_{k=k_\flat}^{2^j - k_\sharp} \tilde{p}_\ell(k)\ \varphi_{j,k}(x) + 2^{j/2}\Phi_\ell^\sharp(2^j(1-x)). \tag{11}$$

Similarly, the biorthogonal spaces $\tilde{V}_j$ are defined with the same structure, allowing the polynomial reproduction up to degree $\tilde{r}-1$:

$$\tilde{V}_j = span\{\tilde{\Phi}_{j,\ell}^\flat\}_{\ell=0,\tilde{r}-1} \oplus \tilde{V}_j^{int} \oplus span\{\tilde{\Phi}_{j,\ell}^\sharp\}_{\ell=0,\tilde{r}-1}, \tag{12}$$

where $\tilde{V}_j^{int} = span\{\tilde{\varphi}_{j,k}\ ;\ k = \tilde{k}_\flat,\ 2^j - \tilde{k}_\sharp\}$ is the space generated by interior scaling functions $\tilde{\varphi}_{j,k}(x) = 2^{j/2}\tilde{\varphi}^1(2^j x - k)$, whose supports are included into $[\frac{\tilde{\delta}_\flat}{2^j}, 1 - \frac{\tilde{\delta}_\sharp}{2^j}]$ ($\tilde{\delta}_\flat,\ \tilde{\delta}_\sharp \in \mathbb{N}$ be two parameters). The edge scaling functions at 0 are defined by:

$$0 \leq \ell \leq \tilde{r}-1, \quad \tilde{\Phi}_\ell^\flat(x) = \sum_{k=1-\tilde{n}_{max}}^{\tilde{k}_\flat - 1} p_\ell(k)\ \tilde{\varphi}(x-k)\ \chi_{[0,+\infty[}.$$

The equality between dimensions of V_j and $\tilde{V}_j$ is obtained by adjusting the parameters $\tilde{\delta}_\flat = \tilde{k}_\flat - \tilde{n}_{max}$ and $\tilde{\delta}_\sharp = \tilde{k}_\sharp + \tilde{n}_{min}$ (with $[\tilde{n}_{min}, \tilde{n}_{max}] = supp\ \tilde{\varphi}$) such that: $\Delta_j = \dim(V_j) = \dim(\tilde{V}_j) = 2^j - (\delta_\flat + \delta_\sharp) - (n_{max} - n_{min}) + 2r + 1$. Remark that $(\delta_\flat,\ \delta_\sharp)$ remain "free" parameters of the construction (often chosen equal to 0 or 1). The last step of the construction lies in the biorthogonalization process of the basis functions, since edge scaling functions of V_j and $\tilde{V}_j$ are no more biorthogonal [1,8,12,17]. Finally, the spaces $(V_j, \tilde{V}_j)$ form a biorthogonal MRA of $L^2(0,1)$.

2.1 Boundary conditions

A multiresolution analyses of $H_0^m(0,1) = \{f \in H^m(0,1)\ :\ f^{(p)}(0) = f^{(p)}(1) = 0,\ \ 0 \le p \le m-1\}$ can be defined from V_j by taking $V_j^{m,0} = V_j \cap H_0^m(0,1)$. For instance, if $m = 1$, as described in [16,17], it suffices to remove the edge scaling functions $\Phi_0^\flat$ at edge 0 and $\Phi_0^\sharp$ at edge 1 which leads to:

$$V_j^{1,0} = span\{\Phi_{j,\ell}^\flat\ ;\ \ell = 1, r-1\} \oplus V_j^{int} \oplus span\{\Phi_{j,\ell}^\sharp\ ;\ \ell = 1, r-1\}.$$

In such case, we also remove the edge functions $\tilde{\Phi}_0^\flat$ and $\tilde{\Phi}_0^\sharp$ from $\tilde{V}_j$ prior to biorthogonalization, to adjust the dimension of the biorthogonal space. Then, the spaces $(V_j^{1,0}, \tilde{V}_j^{1,0})$ constitute a biorthogonal multiresolution analyses of $H_0^1(0,1)$.

3 Construction of $(V_j^0, \tilde{V}_j^0)$ linked by differentiation / integration with $(V_j^1, \tilde{V}_j^1)$

The construction of biorthognal multiresolution analysis of $L^2(0,1)$ linked by differentiation/ integration is based on the following proposition of Lemarié-Rieusset [15]:

Proposition 1 *Let $(V_j^1(\mathbb{R}))$ be a MRA of $L^2(\mathbb{R})$, with differentiable and compactly supported scaling function $\varphi^1 \in \mathcal{C}^{1+\epsilon}$ and wavelet ψ^1. Then there exists a MRA $(V_j^0(\mathbb{R}))$, with associated scaling function φ^0 and wavelet ψ^0, such that:*
$(\varphi^1)'(x) = \varphi^0(x)\ -\ \varphi^0(x-1)$ and $(\psi^1)'\ =\ 4\ \psi^0$.
The biorthogonal functions verify: $\int_x^{x+1} \tilde{\varphi}^1(t)\ dt = \tilde{\varphi}^0(x)$ and $(\tilde{\psi}^0)'\ =\ -4\ \tilde{\psi}^1$.

From the generators $(\varphi^1, \tilde{\varphi}^1)$, $(\varphi^0, \tilde{\varphi}^0)$ of Proposition 1, Jouini and Lemarié-Rieusset prove the existence of two one-dimensional MRA of $L^2(0,1)$, denoted (V_j^1) and (V_j^0) linked by differentiation [14]:

$$\frac{d}{dx} V_j^1 = V_j^0. \tag{13}$$

Moreover, the biorthogonal spaces should satisfy:

$$\tilde{V}_j^0 = H_0^1(0,1) \cap \int_0^x \tilde{V}_j^1 = \left\{ f\ :\ f' \in \tilde{V}_j^1 \text{ and } \ f(0) = f(1) = 0 \right\}. \tag{14}$$

The construction of Jouini and Lemarié-Rieusset [14] remains in a theoretical setting based on the use of Daubechies compactly supported orthogonal generators

[9]. A construction that uses classical biorthogonal multiresolution analyses on the interval [4,8,12], with polynomial reproduction at boundaries, was done and implemented by Kadri-Harouna and Perrier [18]. In such a construction, the choice of integer parameters $(\delta_\flat, \delta_\sharp)$ is very important: they must be identical for the two multiresolutions analyses to satisfy (13,14) and to provide the commutation of multiscal projector with the derivation operator.

Precisely, let $(V_j^1, \tilde{V}_j^1)$ be a BMA of $L^2(0,1)$ with polynomial reproduction up to degree $(r-1, \tilde{r}-1)$ constructed from scaling functions $(\varphi^1, \tilde{\varphi}^1)$ and integer parameters $(\delta_\flat, \delta_\sharp)$ and $(\tilde{\delta}_\flat, \tilde{\delta}_\sharp)$, respectively. Following the same construction, the BMA $(V_j^0, \tilde{V}_j^0)$ of $L^2(0,1)$ constructed with $(\varphi^0, \tilde{\varphi}^0)$ arising from Proposition 1 and $(\delta_\flat, \delta_\sharp)$ and $(\tilde{\delta}_\flat, \tilde{\delta}_\sharp)$ has $(r-2, \tilde{r})$ polynomial reproduction and satisfy:

Proposition 2 *The biorthogonal spaces $(V_j^1, \tilde{V}_j^1)$ and $(V_j^0, \tilde{V}_j^0)$ verify relations (13, 14): $\frac{d}{dx} V_j^1 = V_j^0$ and $\tilde{V}_j^0 = H_0^1 \cap \int_0^x \tilde{V}_j^1$.*

This result induces the commutation between multiscale projectors and differentiation operator. Indeed, let $\mathcal{P}_j^1$ be the oblique projector on V_j^1 parallel to $(\tilde{V}_j^1)^\perp$, $\tilde{\mathcal{P}}_j^1$ its adjoint, and $\mathcal{P}_j^0$, $\tilde{\mathcal{P}}_j^0$ the biorthogonal projectors associated with $(V_j^0, \tilde{V}_j^0)$, we have [14]:

Proposition 3
(i) $\forall\ f \in H^1(0,1),\quad \frac{d}{dx} \circ \mathcal{P}_j^1 f = \mathcal{P}_j^0 \circ \frac{d}{dx} f,$
(ii) $\forall\ f \in H_0^1(0,1),\quad \frac{d}{dx} \circ \tilde{\mathcal{P}}_j^0 f = \tilde{\mathcal{P}}_j^1 \circ \frac{d}{dx} f.$

3.1 Wavelet spaces

We first recall the structure of wavelet spaces of the BMRA $(V_j^1, \tilde{V}_j^1)$, which is classical, although different kinds of wavelets may be designed [1,4,8,12,17]. The biorthogonal wavelet spaces associated to V_j^1 are defined by $W_j^1 = V_{j+1}^1 \cap (\tilde{V}_j^1)^\perp$ and, for $j \geq j_{min}$, have the form: $W_j^1 = W_j^{1,\flat} \oplus W_j^{1,int} \oplus W_j^{1,\sharp}$,

$$\text{with} \begin{cases} W_j^{1,\flat} & = span\{\Psi_{j,\ell}^{1,\flat}(x) = 2^{j/2}\Psi_\ell^{1,\flat}(2^j x)\ ;\ \ell = 0,\ p_\flat - 1\}, \\ W_j^{1,int} & = span\{\psi_{j,k}^1 = 2^{j/2}\psi^1(2^j x - k)\ ;\ k = p_\flat,\ 2^j - p_\sharp - 1\}, \\ W_j^{1,\sharp} & = span\{\Psi_{j,\ell}^{1,\sharp}(1-x) = 2^{j/2}\Psi_\ell^{1,\sharp}(2^j(1-x))\ ;\ \ell = 0,\ p_\sharp - 1\}, \end{cases}$$

$p_\flat$ and $p_\sharp$ are suitable integers to ensure that the support of *interior wavelets* $\psi_{j,k}^1$ of $W_j^{1,int}$ is included into $[\frac{\delta_\flat}{2^{j+1}}, 1 - \frac{\delta_\sharp}{2^{j+1}}]$ (the support of ψ^1 (wavelet on $\mathbb{R}$) is $[\frac{n_{min} - \tilde{n}_{max}+1}{2}, \frac{n_{max} - \tilde{n}_{min}+1}{2}]$). If we follow the construction [12] of *edge wavelets*, we deduce: $p_\flat = \lfloor \frac{\tilde{n}_{max} + k_\flat - 1}{2} \rfloor$ and $p_\sharp = \lfloor \frac{k_\sharp - \tilde{n}_{min}+1}{2} \rfloor$. The biorthogonal spaces $\tilde{W}_j^1$ are constructed in the same way, finally the wavelet bases of the two spaces must to be biorthogonalized identically as the scaling functions. The resulting wavelet bases are denoted by $\{\psi_{j,k}^1\}_{k=1,2^j}$ and $\{\tilde{\psi}_{j,k}^1\}_{k=1,2^j}$ without distinction.
The objective now is to exhibit biorthogonal wavelets of W_j^0 and $\tilde{W}_j^0$, linked to $\psi_{j,k}^1$ and $\tilde{\psi}_{j,k}^1$ by differentiation/integration. This is done by the following proposition, established in the general framework by [14]:

Proposition 4 *Let $(V_j^1, \tilde{V}_j^1)$ and $(V_j^0, \tilde{V}_j^0)$ BMRAs satisfying proposition 2. The wavelet spaces $W_j^0 = V_{j+1}^0 \cap (\tilde{V}_j^0)^\perp$ and $\tilde{W}_j^0 = \tilde{V}_{j+1}^0 \cap (V_j^0)^\perp$ are linked to the biorthogonal wavelet spaces associated to $(V_j^1, \tilde{V}_j^1)$ by:*

$$W_j^0 = \frac{d}{dx} W_j^1 \quad \textit{and} \quad \tilde{W}_j^0 = \int_0^x \tilde{W}_j^1. \tag{15}$$

Moreover, let $\{\psi_{j,k}^1\}_{k=1,2^j}$ and $\{\tilde{\psi}_{j,k}^1\}_{k=1,2^j}$ be two biorthogonal wavelet bases of W_j^1 and $\tilde{W}_j^1$. Biorthogonal wavelet bases of W_j^0 and $\tilde{W}_j^0$ are directly defined by:

$$\psi_{j,k}^0 = 2^{-j} (\psi_{j,k}^1)' \quad \textit{and} \quad \tilde{\psi}_{j,k}^0 = -2^j \int_0^x \tilde{\psi}_{j,k}^1. \tag{16}$$

Interior wavelets $\psi_{j,k}^0(x) = 2^{j/2}\psi^0(2^j x - k)$ in this definition correspond to classical wavelets, ψ^0 being a wavelet on $\mathbb{R}$ associated to the scaling function φ^0 as in Proposition 1. On the other hand, in standard constructions [4,8,17,12], the edge wavelets of W_j^0 and $\tilde{W}_j^0$ do not verify the relations (16).

We now define the change of basis matrices between the spaces $(\frac{d}{dx}V_j^1, \frac{d}{dx}\tilde{V}_j^0)$ and $(V_j^0, \tilde{V}_j^1)$, useful in numerical computations of wavelet filters.

Definition 1 Let $(L_j^1, L_j^0, \tilde{L}_j^0)$ be the change of basis matrices defined by:

$$\frac{d}{dx}\varphi_{j,k}^1 = \sum_{n=1}^{\Delta_j - 1} (L_j^1)_{k,n}\ \varphi_{j,n}^0, \qquad \frac{d}{dx}\tilde{\varphi}_{j,k}^0 = \sum_{n=1}^{\Delta_j} (\tilde{L}_j^0)_{k,n}\ \tilde{\varphi}_{j,n}^1, \tag{17}$$

$$\text{and} \qquad -\int_0^x \varphi_{j,k}^0 = \sum_{m=1}^{\Delta_j} (L_j^0)_{k,m}\ \varphi_{j,m}^1. \tag{18}$$

Remark 1 The matrices L_j^0 and $\tilde{L}_j^0$ are rectangular of size $(\Delta_j - 1) \times \Delta_j$. The biorthogonality between V_j^0 and $\tilde{V}_j^0$, and the inclusion $\tilde{V}_j^0 \subset H_0^1(0,1)$ lead to: $L_j^0(\tilde{L}_j^0)^T = \tilde{L}_j^0(L_j^0)^T = I_{(\Delta_j - 1)}$, where $I_{(n)}$ denotes the identity matrix of size n.

The next proposition guarantees that this new edge wavelets preserve fast algorithms since they satisfy two-scale equations.

Proposition 5 *Let $\{\psi_{j,k}^1\}_{k=1,2^j}$ and $\{\tilde{\psi}_{j,k}^1\}_{k=1,2^j}$ be two biorthogonal wavelet bases of W_j^1 and $\tilde{W}_j^1$ associated respectively to filters G_j^1 and $\tilde{G}_j^1$:*

$$\psi_{j,k}^1 = \sum_n (G_j^1)_{k,n}\ \varphi_{j+1,n}^1 \quad \textit{and} \quad \tilde{\psi}_{j,k}^1 = \sum_n (\tilde{G}_j^1)_{k,n}\ \tilde{\varphi}_{j+1,n}^1.$$

Then there exist sparse matrices G_j^0 and $\tilde{G}_j^0$ defined by:

$$G_j^0 = 2^{-j} G_j^1 L_{j+1}^1 \quad \textit{and} \quad \tilde{G}_j^0 = -2^j \tilde{G}_j^1 L_{j+1}^{0T}, \tag{19}$$

such that the wavelets $\psi_{j,k}^0$ and $\tilde{\psi}_{j,k}^0$ satisfy:

$$\psi_{j,k}^0 = \sum_n (G_j^0)_{k,n} \varphi_{j+1,n}^0 \quad \textit{and} \quad \tilde{\psi}_{j,k}^0 = \sum_n (\tilde{G}_j^0)_{k,n} \tilde{\varphi}_{j+1,n}^0.$$

Proof From the definition of wavelets (16) and of the change of basis (definition 1):

$$2^j \psi^0_{j,k} = \sum_n (G^1_j)_{k,n} (\varphi^1_{j+1,n})' = \sum_{n,m} (G^1_j)_{k,n} (L^1_{j+1})_{n,m} \varphi^0_{j+1,m} = \sum_m [G^1_j L^1_{j+1}]_{k,m} \varphi^0_{j+1,m},$$

since $\psi^0_{j,k} = \sum_m (G^0_j)_{k,m} \varphi^0_{j+1,m}$, we obtain G^0_j. $\tilde{G}^0_j$ is obtained similarly.

4 New construction of $(V^1_j, \tilde{V}^1_j)$ linked to $(V^0_j, \tilde{V}^0_j)$ by differentiation / integration

In this section we present our new construction of biorthogonal multiresolution analyses linked by differentiation and integration. The construction of the primal spaces (V^1_j, V^0_j) remains the same as in the classical construction [14,18]. However, the construction of the biorthogonal spaces $(\tilde{V}^1_j, \tilde{V}^0_j)$ and the wavelet bases will be different.

The construction starts with $(V^0_j, \tilde{V}^0_j)$ as a standard biorthogonal multiresolution analyses of $L^2(0,1)$ [1,4,5], where the scaling functions generators $(\varphi^0, \tilde{\varphi}^0)$ satisfy Proposition 1. Again, we denote by $(\delta_\flat, \delta_\sharp)$ and $(\tilde{\delta}_\flat, \tilde{\delta}_\sharp)$ the integer parameters used in the construction of $(V^0_j, \tilde{V}^0_j)$. Following [14,18], the classical multiresolution spaces V^1_j constructed from the scaling function φ^1 with the same integer parameters $(\delta_\flat, \delta_\sharp)$ satisfy:

$$\frac{d}{dx} V^1_j = V^0_j \quad \text{and} \quad \Delta^1_j - 1 = \Delta^0_j.$$

In this case, for the biorthogonal space $\tilde{V}^0_j$, since $\Delta^0_j = dim(\tilde{V}^0_j)$, we see that:

$$\Delta^1_j - 2 = dim(\frac{d}{dx} \tilde{V}^0_j).$$

The construction of $\tilde{V}^1_j$ follows similar approach. To get equality between dimensions of spaces V^1_j and $\tilde{V}^1_j$:

$$\Delta^1_j = \tilde{\Delta}^1_j,$$

the integer parameters to be used for the construction of $\tilde{V}^1_j$ must be fixed to $(\tilde{\delta}_\flat - 1, \tilde{\delta}_\sharp - 1)$. It follows therefore that:

$$\frac{d}{dx} \tilde{V}^0_j \not\subset \tilde{V}^1_j.$$

This is another difference compared to the existing construction.

The construction of the wavelet basis associated to V^1_j is the major contribution of the present work. In the classical construction, on defines the wavelet space as:

$$V^1_{j+1} = V^1_j \oplus W^1_j, \quad \text{where} \quad W^1_j = V^1_{j+1} \cap (\tilde{V}^1_j)^\perp.$$

Then, the space W_j^1 does not necessarily satisfy homogeneous Dirichlet boundary condition. To compensate for that, in this work the wavelet spaces are defined as:

$$\overline{W}_j^1 = \int_0^x W_j^0,$$

where W_j^0 is the wavelet space associated to V_j^0 [1,4,8,12,17]:

$$W_j^0 = V_{j+1}^0 \cap (\tilde{V}_j^0)^{\perp}.$$

Remark 2
From the zeros mean value property of the wavelet $\psi_{j,k}^0$, by construction the space $\overline{W}_j^1$ satisfies:

$$\overline{W}_j^1 \subset H_0^1(0,1).$$

In the previous section, the wavelet space W_j^0 is defined as $W_j^0 = \frac{d}{dx} W_j^1$ and this choice of W_j^0 leads in general to:

$$W_j^1 \neq \int_0^x W_j^0.$$

For all $j \geq j_{min}$, the spaces $\overline{W}_j^1$ verify the following proposition:

Proposition 6
Let W_j^0 be the wavelet space associated to V_j^0, where $V_j^0 = \frac{d}{dx} V_j^1$. Then the space V_{j+1}^1 can be decomposed as follows:

$$V_{j+1}^1 = V_j^1 \oplus \overline{W}_j^1, \quad \textit{with} \quad \overline{W}_j^1 = \int_0^x W_j^0. \tag{20}$$

and

$$V_{j+1}^1 = V_{j_{min}}^1 \oplus \overline{W}_{j_{min}}^1 \oplus \cdots \oplus \overline{W}_j^1. \tag{21}$$

Proof As $\frac{d}{dx} V_j^1 = V_j^0$, we get:

$$\overline{W}_j^1 = \int_0^x W_j^0 \subset \int_0^x \frac{d}{dt} V_{j+1}^1 \subset V_{j+1}^1 \quad \text{and} \quad \int_0^x W_j^0 \subset H_0^1(0,1).$$

Moreover, let u_j be a function of $V_j^1 \cap \overline{W}_j^1$:

$$u_j = \sum_k c_k \varphi_{j,k}^1 = \sum_n d_n \int_0^x \psi_{j,n}^0,$$

we deduce that:

$$\frac{d}{dx} u_j \in V_j^0 \cap W_j^0 \;\Rightarrow\; \frac{d}{dx} u_j = 0 \;\Rightarrow\; u_j = C \in \mathbb{R}.$$

Since

$$\langle 1, \int_0^x \psi_{j,n}^0 \rangle = -\langle x, \psi_{j,n}^0 \rangle = 0,$$

we get $u_j = 0$, which implies $V_j^1 \cap \overline{W}_j^0 = \{0\}$. Let $f_{j+1} \in V_{j+1}^1$, then:

$$\frac{d}{dx} f_{j+1} \in V_{j+1}^0 = V_j^0 \oplus W_j^0.$$

Since $f_{j+1}(0) \in V_j^1$, integration gives:

$$f_{j+1}(x) = f_{j+1}(0) + \int_0^x \mathcal{P}_j^0(\frac{d}{dx} f_{j+1}) + \int_0^x \mathcal{Q}_j^0(\frac{d}{dx} f_{j+1}) \in V_j^1 + \overline{W}_j^1,$$

and this ends the proof.

The interest of such a wavelet space construction is that homogeneous Dirichlet boundary condition can be handled easily. Indeed, by construction the space $\overline{W}_j^1 \subset H_0^1(0,1)$ and relation (21) allows to get the following decomposition:

$$V_{j+1}^{1,0} = V_{j+1}^1 \cap H_0^1(0,1) = V_{j_{min}}^1 \cap H_0^1(0,1) \oplus \overline{W}_{j_{min}}^1 \oplus \cdots \oplus \overline{W}_j^1.$$

Moreover, if we define $\tilde{V}_j^{1,0}$ as $\tilde{V}_j^{1,0} = \frac{d}{dx}\tilde{V}_j^0$, we have:

Proposition 7
Let $(V_j^1, \tilde{V}_j^1)$ and $(V_j^0, \tilde{V}_j^0)$ be two BMRAs of $L^2(0,1)$ linked by differentiation and integration such that:

$$\frac{d}{dx} V_j^1 = V_j^0 \quad \textit{and} \quad \frac{d}{dx}\tilde{V}_j^0 = \tilde{V}_j^{1,0} \subset L^2(0,1), \tag{22}$$

where $V_j^{1,0}$ is the multiresolution analysis of $H_0^1(0,1)$ provided by $V_j^{1,0} = V_j^1 \cap H_0^1(0,1)$. Then, the wavelet space $\int_0^x W_j^0$ is the classical wavelet space associated to $V_j^{1,0}$:

$$V_{j+1}^{1,0} = V_{j+1}^1 \cap H_0^1(0,1) = V_j^{1,0} \oplus \int_0^x W_j^0 \quad \textit{and} \quad \int_0^x W_j^0 = V_{j+1}^{1,0} \cap (\tilde{V}_j^{1,0})^\perp. \tag{23}$$

Proof
From the vanishing moment condition of the wavelet basis of W_j^0 we get:

$$\int_0^1 W_j^0 = 0 \quad \Rightarrow \quad \int_0^x W_j^0 \subset H_0^1(0,1).$$

The differentiation relation gives:

$$\frac{d}{dx} V_{j+1}^1 = V_{j+1}^0 \quad \Rightarrow \quad \int_0^x V_{j+1}^0 \subset V_{j+1}^1,$$

thus

$$\int_0^x W_j^0 \subset V_{j+1}^1 \cap H_0^1(0,1) = V_{j+1}^{1,0}.$$

The differentiation relation:

$$\frac{d}{dx}\tilde{V}_j^0 = \tilde{V}_j^{1,0}$$

states that for any $\tilde{f}_j^{1,0} \in \tilde{V}_j^{1,0}$, there exists $\tilde{f}_j^0 \in \tilde{V}_j^0$ such that $(\tilde{f}_j^0)' = \tilde{f}_j^{1,0}$, then:

$$\langle \int_0^x \psi_{j,k}^0, \tilde{f}_j^{1,0} \rangle = \langle \int_0^x \psi_{j,k}^0, \frac{d}{dx}\tilde{f}_j^0 \rangle = -\langle \psi_{j,k}^0, \tilde{f}_j^0 \rangle = 0 \quad \Rightarrow \quad \int_0^x W_j^0 \subset (\tilde{V}_j^{1,0})^\perp.$$

Then we deduce that $\int_0^x W_j^0 \subset V_{j+1}^{1,0} \cap (\tilde{V}_j^{1,0})^\perp$ and since the two spaces have the same dimension, we get:

$$\int_0^x W_j^0 = V_{j+1}^{1,0} \cap (\tilde{V}_j^{1,0})^\perp.$$

We recall that the integer parameters used in the construction of $\tilde{V}_j^1$ and $\tilde{V}_j^0$ are not the same, thus one can not expect to get commutation between multiscale projectors and derivation as in Proposition 3. However, for the oblique multiscale projectors of $(V_j^{1,0}, V_j^0)$ and $(\tilde{V}_j^0, \tilde{V}_j^{1,0})$, we can prove the following proposition:

Proposition 8
Let $(\mathcal{P}_j^{1,0}, \mathcal{P}_j^0)$ be the biorthogonal projectors associated with $(V_j^{1,0}, V_j^0)$ and $(\widetilde{\mathcal{P}}_j^0, \widetilde{\mathcal{P}}_j^{1,0})$ the biorthogonal projectors associated with $(\tilde{V}_j^0, \tilde{V}_j^{1,0})$. Then, we have:

(i) $\forall\ f \in H_0^1(0,1), \quad \frac{d}{dx} \circ \mathcal{P}_j^{1,0} f = \mathcal{P}_j^0 \circ \frac{d}{dx} f.$
(ii) $\forall\ f \in H^1(0,1), \quad \frac{d}{dx} \circ \tilde{\mathcal{P}}_j^0 f = \tilde{\mathcal{P}}_j^{1,0} \circ \frac{d}{dx} f.$

Proof
From proposition 7, there are two matrices denoted $L_j^{1,0}$ and $\widetilde{L}_j^{1,0}$ of size $(\Delta_j^1 - 2) \times (\Delta_j^1 - 1)$, such that:

$$\varphi_{j,k}^{1,0} = \sum_{n=1}^{\Delta_j^1 - 1} (L_j^{1,0})_{k,n} \int_0^x \varphi_{j,n}^0 \qquad \text{and} \qquad \tilde{\varphi}_{j,k}^{1,0} = \sum_{n=1}^{\Delta_j^1 - 1} (\widetilde{L}_j^{1,0})_{k,n} \frac{d}{dx} \tilde{\varphi}_{j,n}^0.$$

The biorthogonality of the basis functions $\varphi_{j,k}^{1,0}$ and $\tilde{\varphi}_{j,k}^{1,0}$, with an integration by part give:

$$\begin{aligned}\delta_{k,m} = \langle \varphi_{j,k}^{1,0}, \tilde{\varphi}_{j,m}^{1,0} \rangle &= \sum_\ell (\widetilde{L}_j^{1,0})_{m,\ell} \langle \varphi_{j,k}^{1,0}, \frac{d}{dx} \tilde{\varphi}_{j,\ell}^0 \rangle = \sum_\ell (\widetilde{L}_j^{1,0})_{m,\ell} \langle -\frac{d}{dx} \varphi_{j,k}^{1,0}, \tilde{\varphi}_{j,\ell}^0 \rangle \\ &= -\sum_n \sum_\ell (L_j^{1,0})_{k,n} (\widetilde{L}_j^{1,0})_{m,\ell} \langle \varphi_{j,n}^0, \tilde{\varphi}_{j,\ell}^0 \rangle = -\sum_n (L_j^{1,0})_{k,n} (\widetilde{L}_j^{1,0})_{m,n},\end{aligned}$$

which means that:

$$I_{\Delta_j - 2} = -L_j^{1,0}\ {}^t\widetilde{L}_j^{1,0}.$$

Thus, the proof of the point (i) becomes a change of basis. Indeed, for $f \in H_0^1(0,1)$, we have:

$$\begin{aligned}\frac{d}{dx} \mathcal{P}_j^{1,0}(f) &= \sum_k \langle f, \tilde{\varphi}_{j,k}^{1,0} \rangle\ \frac{d}{dx} \varphi_{j,k}^{1,0} = \sum_k \sum_n (L_j^{1,0})_{k,n} \langle f, \tilde{\varphi}_{j,k}^{1,0} \rangle\ \varphi_{j,n}^0 \\ &= \sum_n \langle f, \sum_k (L_j^{1,0})_{k,n} \tilde{\varphi}_{j,k}^{1,0} \rangle\ \varphi_{j,n}^0 = \sum_n \langle f, \sum_k \sum_m (L_j^{1,0})_{k,n} (\widetilde{L}_j^{1,0})_{k,m} \frac{d}{dx} \tilde{\varphi}_{j,m}^0 \rangle\ \varphi_{j,n}^0 \\ &= \sum_n \langle f, -\frac{d}{dx} \tilde{\varphi}_{j,n}^0 \rangle\ \varphi_{j,n}^0 = \sum_n \langle \frac{d}{dx} f, \tilde{\varphi}_{j,n}^0 \rangle\ \varphi_{j,n}^0 = \mathcal{P}_j^0 (\frac{d}{dx} f).\end{aligned}$$

For the second point (ii), let us consider the matrix $\widetilde{L}_j^0$ defined by:

$$\frac{d}{dx} \tilde{\varphi}_{j,k}^0 = \sum_{n=1}^{\Delta_j^0 - 1} (\widetilde{L}_j^0)_{k,n}\ \tilde{\varphi}_{j,n}^{1,0}.$$

Again, the duality of the basis and integration by part give:

$$\langle \frac{d}{dx}\varphi^{1,0}_{j,k}, \tilde{\varphi}^{0}_{j,m}\rangle = (L^{1,0}_j)_{k,m} = \langle \varphi^{1,0}_{j,k}, -\frac{d}{dx}\tilde{\varphi}^{0}_{j,m}\rangle = -(\tilde{L}^{0}_j)_{m,k},$$

then

$$\begin{aligned}\frac{d}{dx}\tilde{\mathcal{P}}^0_j(f) &= \sum_k \langle f, \varphi^0_{j,k}\rangle \ \frac{d}{dx}\tilde{\varphi}^0_{j,k} = \sum_k\sum_n (\tilde{L}^0_j)_{k,n}\langle f, \varphi^0_{j,k}\rangle \ \tilde{\varphi}^{1,0}_{j,n} \\ &= \sum_n \langle f, \sum_k (\tilde{L}^0_j)_{k,n}\varphi^0_{j,k}\rangle \ \tilde{\varphi}^{1,0}_{j,n} = \sum_n \langle f, -\sum_k (\tilde{L}^{1,0}_j)_{n,k}\varphi^0_{j,k}\rangle \ \tilde{\varphi}^{1,0}_{j,n} \\ &= \sum_n \langle f, -\frac{d}{dx}\varphi^{1,0}_{j,n}\rangle \ \tilde{\varphi}^{1,0}_{j,n} = \sum_n \langle \frac{d}{dx}f, \varphi^{1,0}_{j,n}\rangle \ \tilde{\varphi}^{1,0}_{j,n} = \tilde{\mathcal{P}}^{1,0}_j(\frac{d}{dx}f).\end{aligned}$$

5 Fast decomposition algorithm

In this section we provide numerical algorithms for the computation of the projection of $f_{j+1} \in V^1_{j+1}$ onto V^1_j and $\overline{W}^1_j$ respectively. Precisely, starting with:

$$f_{j+1} = \sum_{k=1}^{\Delta^1_{j+1}} c_{j+1,k}\varphi^1_{j+1,k},$$

we want to compute the coefficients $c_{j,k}$ and $d_{j,k}$ from $c_{j+1,k}$ such that:

$$f_{j+1} = \sum_{k=1}^{\Delta^1_{j+1}} c_{j+1,k}\varphi^1_{j+1,k} = \sum_{k=1}^{\Delta^1_j} c_{j,k}\varphi^1_{j,k} + \sum_{m=1}^{2^j} d_{j,m}\int_0^x \psi^0_{j,m}.$$

Firstly, we notice that f_{j+1} can be splitted as

$$f_{j+1} = \sum_{k=1}^{\Delta^1_{j+1}} c_{j+1,k}\varphi^1_{j+1,k} = f^0_{j+1} + f^{1,0}_{j+1} + f^1_{j+1},$$

with

$$f^0_{j+1} = c_{j+1,1}\varphi^1_{j+1,1} \quad \Rightarrow \quad f^0_{j+1}(0) \neq 0 \ \text{ and } \ f^0_{j+1}(1) = 0,$$

$$f^1_{j+1} = c_{j+1,\Delta^1_{j+1}}\varphi^1_{j+1,\Delta^1_{j+1}} \quad \Rightarrow \quad f^1_{j+1}(0) = 0 \ \text{ and } \ f^1_{j+1}(1) \neq 0,$$

and

$$f^{1,0}_{j+1} = \sum_{k=2}^{\Delta^1_{j+1}-1} c_{j+1,k}\varphi^1_{j+1,k} \in H^1_0(0,1).$$

Then, the function $f^{1,0}_{j+1}$ belongs to $V^{1,0}_{j+1}$ and this space corresponds to:

$$V^{1,0}_{j+1} = V^{1,0}_j \oplus W^{1,0}_j, \ \text{ with } \ W^{1,0}_j = \overline{W}^1_j.$$

Thus, the two scales decomposition of $f_{j+1}^{1,0}$ is a classical decomposition in the multiresolution analysis of $H_0^1(0,1)$ provided by the scaling function filter of $V_j^{1,0}$ and wavelet filter of $W_j^{1,0}$. The projection of f_{j+1}^0 is based on the following two scales relations satisfied by the scaling function $\varphi_{j+1,1}^1$:

$$\varphi_{j+1,1}^1 = \sum_{n=1}^{\tilde{\Delta}_j^1} \tilde{H}_{n,1}^1 \varphi_{j,n}^1 + \sum_{m=1}^{2^j} \tilde{G}_{m,1}^1 \psi_{j,m}^1 = \sum_{n=1}^{\tilde{\Delta}_j^1} \tilde{\overline{H}}_{n,1}^1 \varphi_{j,n}^1 + \sum_{m=1}^{2^j} \tilde{\overline{G}}_{m,1}^1 \int_0^x \psi_{j,m}^0,$$

where the first decomposition corresponds to $V_{j+1}^1 = V_j^1 \oplus W_j^1$ and the second one corresponds to $V_{j+1}^1 = V_j^1 \oplus \overline{W}_j^1$. To get the new filters $\tilde{\overline{H}}_{n,1}^1$ and $\tilde{\overline{G}}_{n,1}^1$, according to the biorthogonalization procedure that we adopted, where only the dual basis are modified, we have:

$$\tilde{G}_{k,1}^1 = \sum_{m=1}^{2^j} \tilde{\overline{G}}_{m,1}^1 \langle \int_0^x \psi_{j,m}^0, \tilde{\psi}_{j,k}^1 \rangle, \tag{24}$$

and

$$\tilde{H}_{k,1}^1 = \tilde{\overline{H}}_{k,1}^1 + \sum_{m=1}^{2^j} \tilde{\overline{G}}_{m,1}^1 \langle \int_0^x \psi_{j,m}^0, \tilde{\varphi}_{j,k}^1 \rangle. \tag{25}$$

Equations (24) and (24) define two linear systems with respect to the edge scaling function and wavelet filters $\tilde{\overline{G}}_{n,1}^1$ and $\tilde{\overline{H}}_{n,1}^1$. From [2,19], the computation of coefficients $\langle \int_0^x \psi_{j,m}^0, \tilde{\psi}_{j,k}^1 \rangle$ and $\langle \int_0^x \psi_{j,m}^0, \tilde{\varphi}_{j,k}^1 \rangle$ is straightforward and this is done only for functions that support intersect the edge function support, due to the compactly support properties of the generators. Then, solving these linear systems, with similar relations at the boundary 1, allows to get the new edge filters. The main steps of the decomposition algorithm are summarized as:

$$\begin{aligned}
c_{j,1} &= c_{j+1,1} \tilde{\overline{H}}_{1,1}^1, \\
c_{j,k} &= \sum_{n=2}^{\Delta_{j+1}-1} c_{j+1,n} \tilde{H}_{n,k}^{1,0} + c_{j+1,1} \tilde{\overline{H}}_{k,1}^1 + c_{j+1,\Delta_{j+1}} \tilde{\overline{H}}_{k,\Delta_{j+1}}^1, \quad 2 \le k \le \Delta_j - 1, \\
c_{j,\Delta_j} &= c_{j+1,\Delta_{j+1}} \tilde{\overline{H}}_{\Delta_j,\Delta_{j+1}}^1,
\end{aligned}$$

and

$$d_{j,k} = \sum_{n=2}^{\Delta_{j+1}-1} c_{j+1,n} \tilde{G}_{n,k}^{1,0} + c_{j+1,1} \tilde{\overline{G}}_{k,1}^1 + c_{j+1,\Delta_{j+1}} \tilde{\overline{G}}_{k,\Delta_{j+1}}^1, \quad 1 \le k \le 2^j.$$

5.1 Fast reconstruction algorithm

For $f_{j+1} \in V_{j+1}^1$, let us suppose that we know its projection onto $V_j^1 \oplus \overline{W}_j^1$ in terms of:

$$f_{j+1} = \sum_{k=1}^{\Delta_j^1} c_{j,k} \varphi_{j,k}^1 + \sum_{m=1}^{2^j} d_{j,m} \int_0^x \psi_{j,m}^0,$$

and we want to compute its projection onto V_{j+1}^1 in terms of:

$$f_{j+1} = \sum_{k=1}^{\Delta_{j+1}^1} c_{j+1,k}\varphi_{j+1,k}^1.$$

Setting

$$\sum_{k=1}^{\Delta_j^1} c_{j,k}\varphi_{j,k}^1 = f_j^0 + f_j^{1,0} + f_j^1, \quad \text{with} \quad f_j^0 = c_{j,1}\varphi_{j,1}^1 \quad \text{and} \quad f_j^1 = c_{j,\Delta_j^1}\varphi_{j,\Delta_j^1}^1,$$

it is easy to see that

$$f_j^{1,0} + \sum_{m=1}^{2^j} d_{j,m} \int_0^x \psi_{j,m}^0 \in V_{j+1}^{1,0},$$

thus we get:

$$c_{j+1,k} = \sum_{n=1}^{\Delta_j^1} c_{j,n} H_{n,k}^1 + \sum_{m=1}^{2^j} d_{j,m} \overline{G}_{m,k}^1, \quad 2 \leq k \leq \Delta_{j+1}^1 - 1,$$

and

$$c_{j+1,1} = \sum_{n=1}^{\Delta_j^1} c_{j,n} H_{n,1}^1, \qquad c_{j+1,\Delta_{j+1}^1} = \sum_{n=1}^{\Delta_j^1} c_{j,n} H_{n,\Delta_{j+1}^1}^1.$$

6 Numerical examples

We present in this section numerical examples to illustrate the potential application of this new construction of multiresolution analysis of $L^2(0,1)$ linked by differentiation and integration. We remind that our construction starts with the construction of V_j^0. Here, for the different examples, the scaling function and wavelet generators (φ^0, ψ^0) considered are Daubechies orthogonal generators, with three vanishing moments for the wavelet [9]. The integer parameters of the construction of V_j^0 thus are:

$$r = 3, \quad \delta_\flat = \delta_\sharp = 1, \quad n_{min} = -r + 1 \quad \text{and} \quad n_{max} = r.$$

On Figure 1, we show the plot of the internal scaling function φ^0 and the wavelet ψ^0. The edges orthogonal scaling functions and wavelets are plotted on Figure 2 and Figure 3 respectively. The generators (φ^1, ψ^1) are computed from (φ^0, ψ^0) using the formula:

$$\varphi^1(x) = \int_{x-1}^x \varphi^0(t)dt \qquad \text{and} \qquad \psi^1(x) = 4\int_{-\infty}^x \psi^0(t)dt. \tag{26}$$

The graphs of φ^1 and ψ^1 are plotted on Figure 4, Figure 5 and Figure 6 show the plot of the edges scaling function graphs. The edge wavelet graphs are plotted on Figure 7 and Figure 8. We notice that these edge wavelets satisfy homogeneous

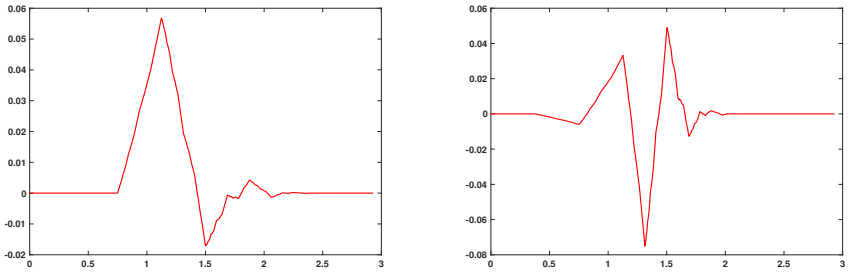

Fig. 1: Plot of the internal scaling function φ^0 (left) and the internal wavelet ψ^0 (right). Daubechies orthogonal generator with $r = 3$.

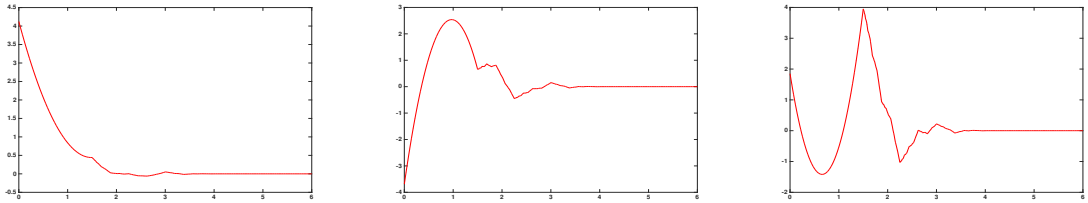

(a) $\Phi_{j,0}^{0,\flat}$ (b) $\Phi_{j,1}^{0,\flat}$ (c) $\Phi_{j,2}^{0,\flat}$

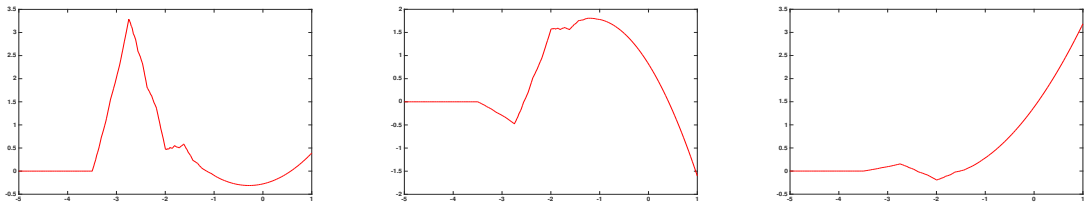

(d) $\Phi_{j,0}^{0,\sharp}$ (e) $\Phi_{j,1}^{0,\sharp}$ (f) $\Phi_{j,2}^{0,\sharp}$

Fig. 2: Plot of the edge orthogonal scaling functions. Daubechies orthogonal generator with $r = 3$.

Dirichlet boundary condition while this boundary condition is not required for all the edge scaling functions.

Similarly, the generators $(\tilde{\varphi}^1, \tilde{\psi}^1)$ biorthogonal to (φ^1, ψ^1) are computed using the formula:

$$\varphi^0(x) = \int_x^{x+1} \tilde{\varphi}^1(t)dt \qquad \text{and} \qquad \psi^0(x) = -4\int_{-\infty}^{x} \tilde{\psi}^1(t)dt. \tag{27}$$

The graphs of $\tilde{\varphi}^1$ and $\tilde{\psi}^1$ are plotted on Figure 9, Figure 10 and Figure 11 show the plot of the edges biorthogonal scaling functions. The edge biorthogonal wavelet graphs are plotted on Figure 12 and Figure 13.

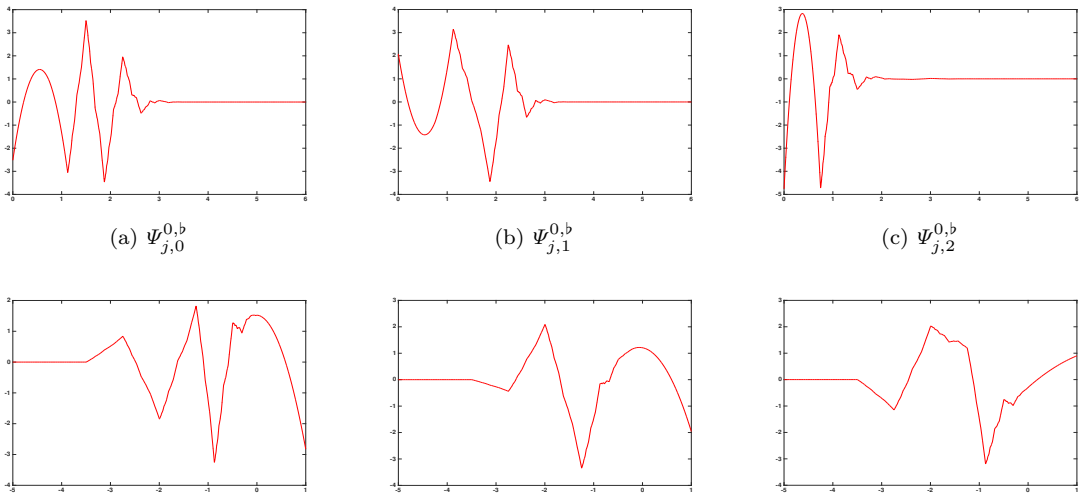

(a) $\Psi_{j,0}^{0,\flat}$ (b) $\Psi_{j,1}^{0,\flat}$ (c) $\Psi_{j,2}^{0,\flat}$

(d) $\Psi_{j,0}^{0,\sharp}$ (e) $\Psi_{j,1}^{0,\sharp}$ (f) $\Psi_{j,2}^{0,\sharp}$

Fig. 3: Plot of the edge orthogonal wavelet functions. Daubechies orthogonal generator with $r = 3$.

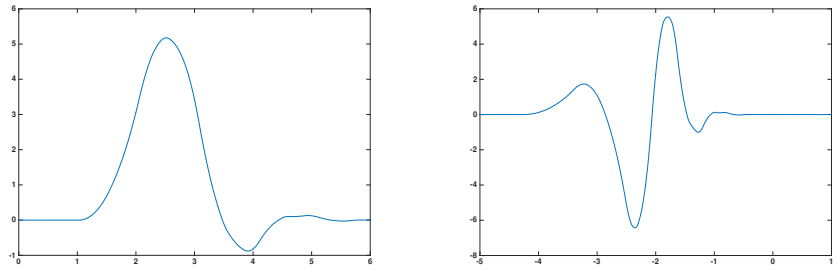

Fig. 4: Plot of the internal scaling function $\varphi^1(x) = \int_{x-1}^{x} \varphi^0(t)dt$ (left) and the internal wavelet $\psi^1(x) = 4\int_{-\infty}^{x} \psi^0(t)dt$ (right), where (φ^0, ψ^0) are Daubechies orthogonal generators with $r = 3$.

We also study the interpolation error of the multiresoltion analysis $(V_j^1, \tilde{V}_j^1)$. For a given function f, which its values are known at grid points $x_k = k/2^{j_{max}}$, $0 \leq k \leq 2^{j_{max}}$, the interpolation step consists of computing the projection

$$\mathcal{P}_{j_{max}}^1(f) = \sum_{k=0}^{\Delta_{j_{max}}^1 - 1} < f, \tilde{\varphi}_{j_{max},k}^1 > \varphi_{j_{max},k}^1. \tag{28}$$

We adapted the quadrature formula and algorithms of [17] to the biorthogonal case to compute numerically the inner product $< f, \tilde{\varphi}_{j_{max},k}^1 >$. For the function f

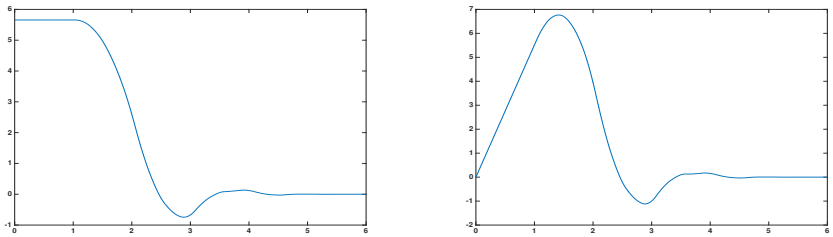

(a) $\Phi^{1,\flat}_{j,0}$ (b) $\Phi^{1,\flat}_{j,1}$

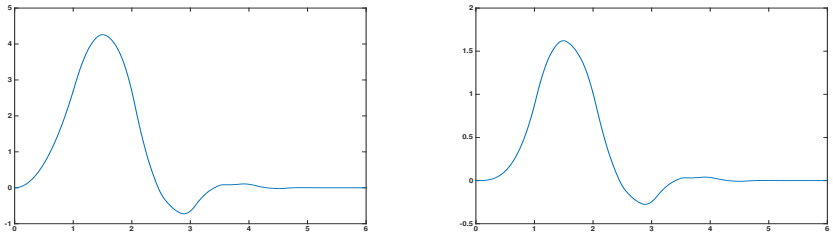

(c) $\Phi^{1,\flat}_{j,2}$ (d) $\Phi^{1,\flat}_{j,3}$

Fig. 5: Plot of the edge scaling functions at edge 0, computed from generator $\varphi^1(x) = \int_{x-1}^{x} \varphi^0(t)dt$, where (φ^0, ψ^0) are Daubechies orthogonal generators with $r = 3$.

defined by:

$$f(x) = \sin(2\pi x)\sin(50x) + 1, \tag{29}$$

we show on Figure 14 the snapshot of the interpolation error $\|f - \mathcal{P}^1_{j_{max}}(f)\|$ according to the different values of j_{max}. Again, from $\tilde{f}_{j_{max}} = \mathcal{P}^1_{j_{max}}(f)$ we study the projection error

$$\|\tilde{f}_{j_{max}} - \mathcal{P}^1_j(\tilde{f}_{j_{max}})\|, \quad j_{min} \leq j \leq j_{max} - 1,$$

involved in the fast wavelet transform algorithm. Figure 15 shows the plot of the projection error in a loglog scale with respect to the resolutions j. The Figure 16 shows the plot of this error at grid points for $j_{max} = 16$ and $j = 9$ or $j = 13$.

To prove the sparse approximation property of the wavelet basis $\psi^1_{j,k}$, we studied the non-linear approximation error of f defined in (29). On Figure 17 we plot the evolution of this error according the ratio of wavelet coefficients retained.

In each of these experiences, the errors decay order obtained is about $s \approx -4$. Since f is very smooth, this is in accordance with the theoretical order which is the polynomial approximation order of the space V^1_j.

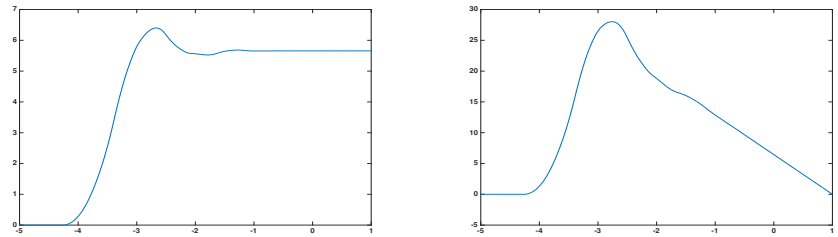

(a) $\Phi^{1,\sharp}_{j,0}$ (b) $\Phi^{1,\sharp}_{j,1}$

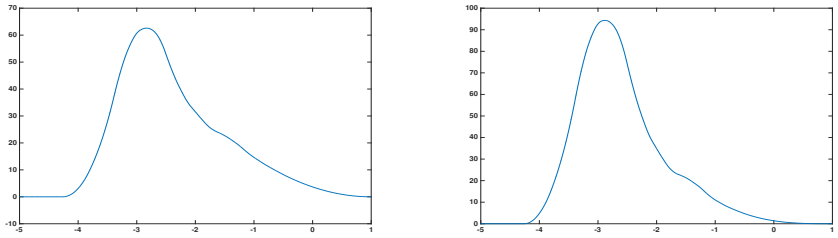

(c) $\Phi^{1,\sharp}_{j,2}$ (d) $\Phi^{1,\sharp}_{j,3}$

Fig. 6: Plot of the edge scaling functions at edge 1, computed from generator $\varphi^1(x) = \int_{x-1}^{x} \varphi^0(t)dt$, where (φ^0, ψ^0) are Daubechies orthogonal generators with $r = 3$.

6.1 One dimensional laplacian operator

In this section, we evaluate the performance of our new wavelet basis construction, in the numerical resolution of one dimension poisson equation with homogeneous Dirichlet boundary condition:

$$\begin{cases} -u''(x) = f(x), \quad x \in]0,1[, \\ u(0) = u(1) = 0. \end{cases} \tag{30}$$

Usually, the numerical resolution of problem (30) with a wavelet based method is done using a Galerkin method. This leads to the resolution of linear algebraic system with the stiffness matrix of the considered wavelet basis [2, 7]. In our construction, the wavelet basis $\psi^0_{j,k}$ can be chosen as an orthogonal basis. In this case, it is easy to see that the stiffness matrix of the wavelet basis $\psi^1_{j,k}$ constructed by integrating $\psi^0_{j,k}$ is a diagonal matrix:

$$< -(\psi^1_{j,k})'', \psi^1_{\ell,n} >=< (\psi^1_{j,k})', (\psi^1_{\ell,n})' >= 2^{j+\ell} < \psi^0_{j,k}, \psi^0_{\ell,n} >= 2^{j+\ell}\delta_{j,\ell}\delta_{k,n}. \tag{31}$$

Then, if the solution u is searched in terms of its wavelet series:

$$u = \sum_{j,k} u_{j,k}\psi^1_{j,k}, \tag{32}$$

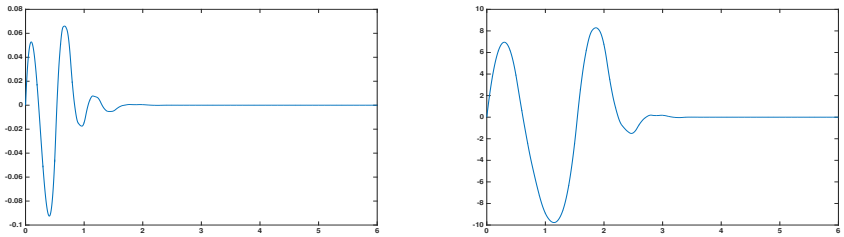

(a) $\Psi^{1,\flat}_{j,0}$ (b) $\Psi^{1,\flat}_{j,1}$

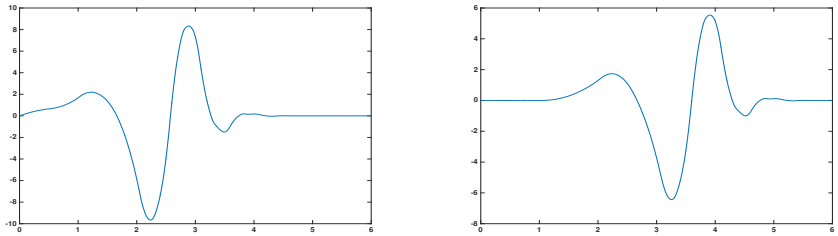

(c) $\Psi^{1,\flat}_{j,2}$ (d) $\Psi^{1,\flat}_{j,3}$

Fig. 7: Plot of the edge wavelet at edge 0, computed from generator $\psi^1(x) = 4\int_{-\infty}^{x} \psi^0(t)dt$, where (φ^0, ψ^0) are Daubechies orthogonal generators with $r = 3$.

the coefficients $u_{j,k}$ are given by:

$$u_{j,k} = 2^{-2j-4} f_{j,k}, \quad \text{where} \quad f = \sum_{j,k} f_{j,k} \tilde{\psi}^1_{j,k}. \tag{33}$$

Thus, the resolution of (30) becomes a wavelet coefficient normalization, which numerical complexity linear. We notice that, at the coarse scale j_{min} we also have to invert the stiffness matrix of the scaling function $\varphi^1_{j_{min},k}$. The size of this matrix is very small compared to the size of the whole system.

To see the efficiency of this approach, we firstly compare its numerical complexity to the complexity of a finite difference method and the multi-grid method of [13]. The main criterion we took is the real computational time of the MATLAB code [] that encodes the method. For this purpose, two numerical experiences have been made. The first experience is done with the exact solution:

$$u(x) = x^3 - x^4. \tag{34}$$

The source term f is appropriately computed from the solution u. On Tab. 1, we provide the different mean real computational time according to the space resolution j. It can be observed that the present method performs better than these two methods when the resolution j increases, with a good accuracy on the relative L_2-error.

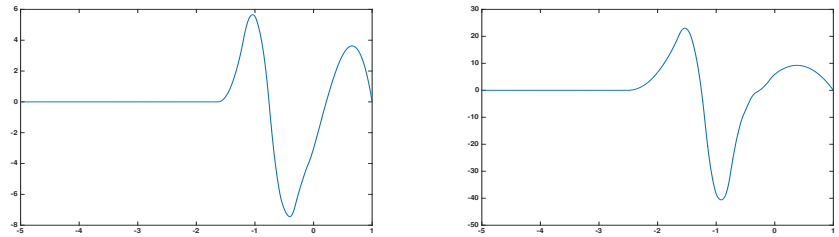

(a) $\Psi^{1,\sharp}_{j,0}$ (b) $\Psi^{1,\sharp}_{j,1}$

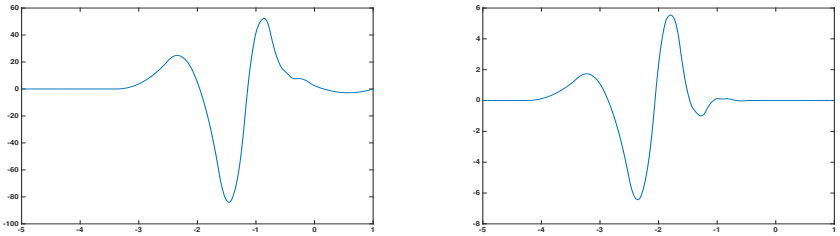

(c) $\Psi^{1,\sharp}_{j,2}$ (d) $\Psi^{1,\sharp}_{j,3}$

Fig. 8: Plot of the edge wavelet at edge 1, computed from generator $\psi^1(x) = 4\int_{-\infty}^{x} \psi^0(t)dt$, where (φ^0, ψ^0) are Daubechies orthogonal generators with $r = 3$.

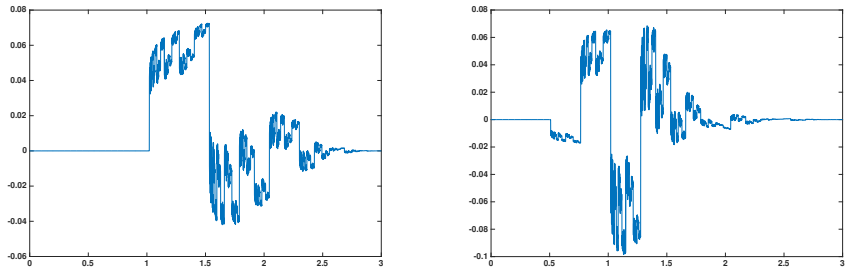

Fig. 9: Plot of the internal scaling function $\tilde{\varphi}^1$ (left) and the internal wavelet $\tilde{\psi}^1(t)$ (right), where (φ^0, ψ^0) are Daubechies orthogonal generators with $r = 3$.

The second experience concerns the source term f defined by:

$$f(x) = \begin{cases} 0, & 0 \leq x < 3/8, \\ 2, & 3/8 \leq x \leq 5/8, \\ 0, & 5/8 < x \leq 1, \end{cases} \tag{35}$$

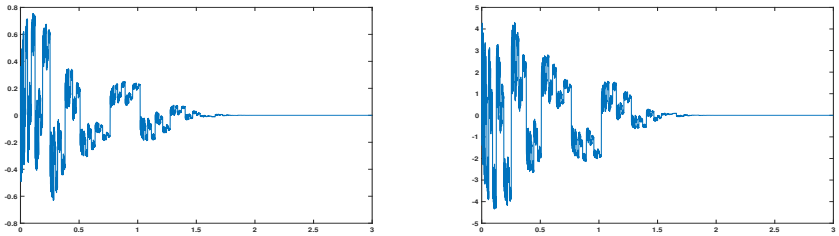

(a) $\tilde{\Phi}^{1,\flat}_{j,0}$ (b) $\tilde{\Phi}^{1,\flat}_{j,1}$

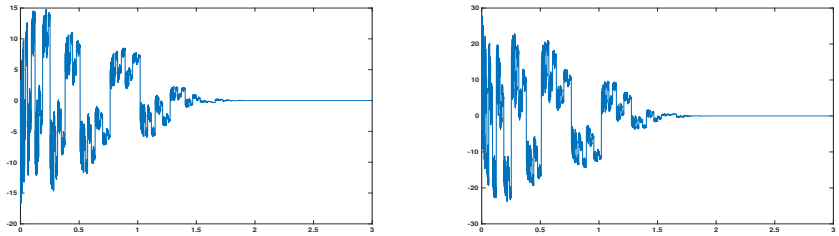

(c) $\tilde{\Phi}^{1,\flat}_{j,2}$ (d) $\tilde{\Phi}^{1,\flat}_{j,3}$

Fig. 10: Plot of the edge biorthogonal scaling functions, where (φ^0, ψ^0) are Daubechies orthogonal generators with $r = 3$.

Computational time			
Method	resolution j	t (seconds)	L_2-error
Multi-grid	8	0.010705	$4.4184E^{-5}$
Present	8	0.000625	$1.3302E^{-9}$
Finite difference	8	0.000205	$4.4341E^{-5}$
Multi-grid	10	0.019202	$2.7255E^{-6}$
Present	10	0.000835	$3.1552E^{-11}$
Finite difference	10	0.000389	$2.7640E^{-6}$
Multi-grid	16	0.089770	$2.0575E^{-7}$
Present	16	0.007712	$5.6942E^{-11}$
Finite difference	16	0.018695	$9.2095E^{-10}$

Table 1: Comparison of the real computational time and the relative L^2-error for the exact solution: $u(x) = x^3 - x^4$.

and this corresponds to an exact solution u of (30) defined by:

$$u(x) = \begin{cases} \frac{1}{4}x, & 0 \le x < 3/8, \\ -x^2 + x - \frac{9}{64}, & 3/8 \le x \le 5/8, \\ -\frac{1}{4}x + \frac{1}{4}, & 5/8 < x \le 1. \end{cases} \tag{36}$$

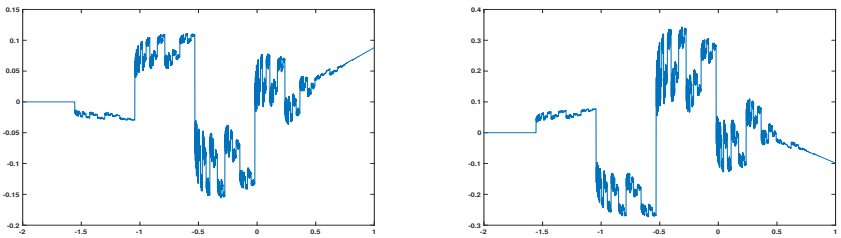

(a) $\tilde{\Phi}^{1,\sharp}_{j,0}$ (b) $\tilde{\Phi}^{1,\sharp}_{j,1}$

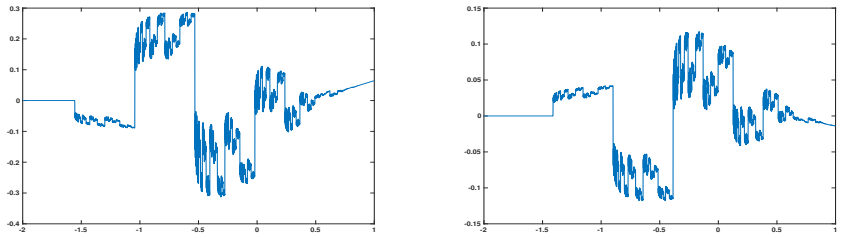

(c) $\tilde{\Phi}^{1,\sharp}_{j,2}$ (d) $\tilde{\Phi}^{1,\sharp}_{j,3}$

Fig. 11: Plot of the edge biorthogonal scaling functions, where (φ^0, ψ^0) are Daubechies orthogonal generators with $r = 3$.

The function f has discontinuities at $x = 3/8$ and $x = 5/8$. Then, the motivation for this experience is to highlight the adaptativity of the wavelet basis $\psi^1_{j,k}$.

7 conclusion

In this paper we have presented a new construction of biorthogonal wavelet bases linked by differentiation and integration. In opposite to the existing construction, the differentiation relation between the wavelets basis $\psi^1_{j,k}$ and $\psi^0_{j,k}$ remains diagonal as for the internal wavelet. To get this point, we have construction a multiresolution analysis of $L^2(0,1)$ for which the wavelet basis satisfy homogeneous Dirichlet boundary condition. Many experiments have demonstrated the potential application of this construction in signal compressing and in the numerical resolution of Poisson equation in one dimensional space.

References

1. L. Andersson, N. Hall, B. Jawerth, G. Peters, Wavelets on closed subsets of the real line, *Recents Advances in Wavelets Analysis (L.L. Schumaker and G. Webb eds)*, Academic Press (1993) 1–61.
2. G. Beylkin, On the representation of operator in bases of compactly supported wavelets, *SIAM J.Numer.Anal.* **6(6)** (1992) 1716–1740.

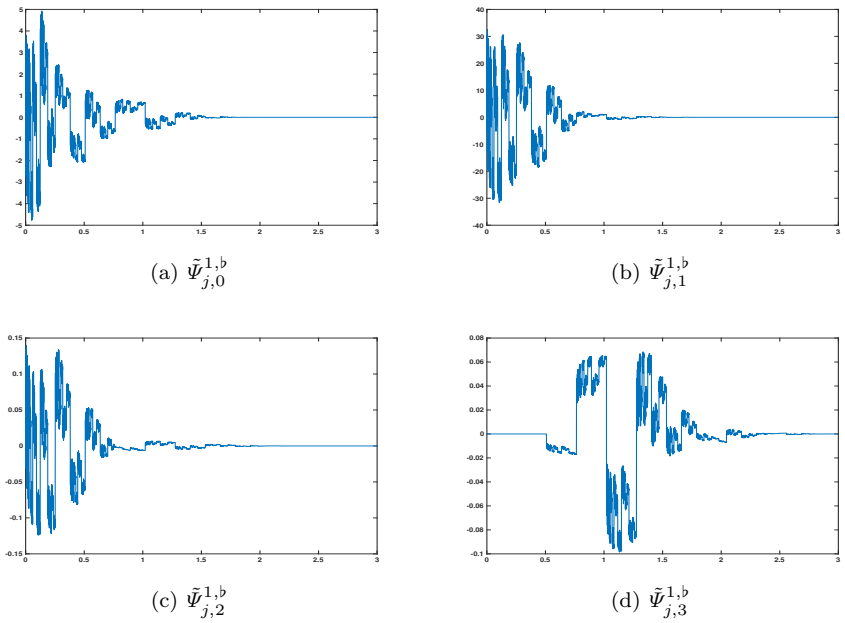

(a) $\tilde{\Psi}^{1,\flat}_{j,0}$ (b) $\tilde{\Psi}^{1,\flat}_{j,1}$

(c) $\tilde{\Psi}^{1,\flat}_{j,2}$ (d) $\tilde{\Psi}^{1,\flat}_{j,3}$

Fig. 12: Plot of the edge biorthogonal wavelets, where (φ^0, ψ^0) are Daubechies orthogonal generators with $r = 3$.

3. C. Canuto, R. Masson, Stabilized wavelet approximations of the Stokes problem, *Math. of Comput.* **70(236)** (2000) 1397–1416.
4. A. Cohen, I. Daubechies, J.-C. Feauveau,Biorthogonal bases of compactly supported wavelets, *Comm. Pure Appli. Maths.* **45** (1992) 485–560.
5. A. Cohen, I. Daubechies, P. Vial, Wavelets on the Interval and Fast Wavelet Transforms, *Appl. Comput. Harmon. Anal.* **1** (1993) 54–81.
6. Z. Cieselski, T. Figiel, Spline bases in classical function spaces on compact manifolds, part II, *Studia Math. LXXVCI* (1983) 95–136.
7. W. Dahmen, A. Kunoth, K. Urban, A wavelet Galerkin method for the stokes equations ,*Computing.* **3 (56)** (1996) 259–301.
8. W. Dahmen, A. Kunoth, K. Urban, Biorthogonal Spline-wavelets on the interval. Stability and moment conditions, *App. Comput. Harmon. Anal.* **6** (1999) 132–196.
9. I. Daubechie, Orthogonal bases of compactly supported wavelets, *Comm. Pure and Appli. Math.* **7 (41)** (1988) 906–996.
10. E. Deriaz, V. Perrier, *Orthogonal Helmholtz decomposition in arbitrary dimension using divergence-free and curl-free wavelets,App. Comput. Harmon. Anal.*, **26** (2009) 249–269.
11. M. Fortin, An analysis of the convergence of mixed finite element methods, *R.A.I.R.O. Anal. Mumer.* **R3 (11)** (1977) 341–354.
12. S. Grivet-Talocia, A. Tabacco, Wavelet on the interval with optimal localization, *Math. Models. Meth. Appl. Sci.* **10(3)** (2000) 441–462.
13. W. Hager, Applied Numerical Linear Algebra, *Prentice-Hall,* (1988).
14. A. Jouini, P.G. Lemarié-Rieusset, Analyse multirésolution biorthogonale sur l'intervalle et applications, *Annales de l'I.H.P. Section C* **10** (1993) 453–476.
15. P.G. Lemarié-Rieusset, Analyses multi-résolutions non orthogonales, commutation entre projecteurs et dérivation et ondelettes vecteurs à divergence nulle, *Revista Matemática Iberoamericana* **8(2)** (1992) 221–236.
16. R. Masson, Biorthogonal spline wavelets on the interval for the resolution of boundary problems, *M3AS.* **6** (6) (1996) 749–791.

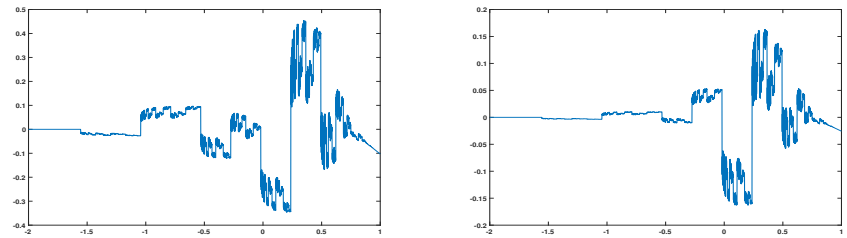

(a) $\tilde{\Psi}^{1,\sharp}_{j,0}$ (b) $\tilde{\Psi}^{1,\sharp}_{j,1}$

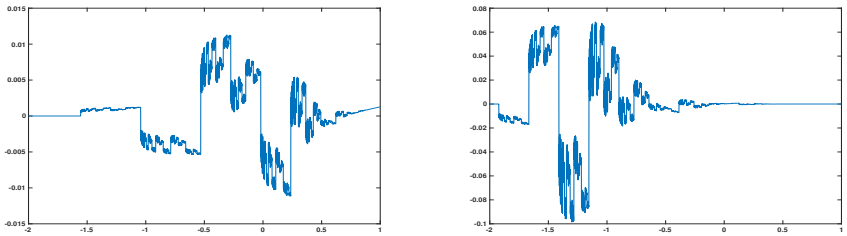

(c) $\tilde{\Psi}^{1,\sharp}_{j,2}$ (d) $\tilde{\Psi}^{1,\sharp}_{j,3}$

Fig. 13: Plot of the edge biorthogonal wavelets, where (φ^0, ψ^0) are Daubechies orthogonal generators with $r = 3$.

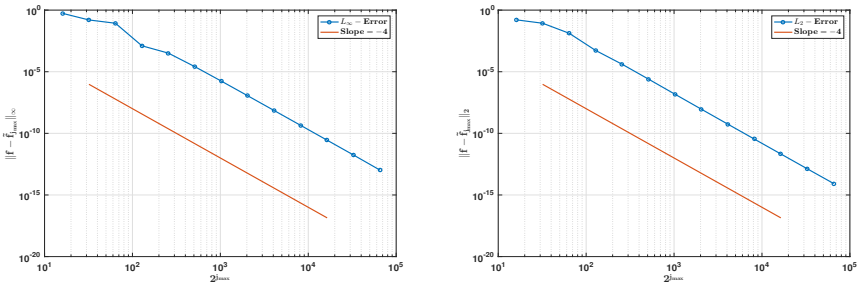

Fig. 14: Plot of the interpolation error $\|f - \tilde{f}_{j_{max}}\|_\infty$ (left) and $\|f - \tilde{f}_{j_{max}}\|_2$ (right) in loglog scale, where (φ^0, ψ^0) are Daubechies orthogonal generators with $r = 3$.

17. P. Monasse, V. Perrier, Orthogonal Wavelet Bases Adapted For Partial Differential Equations With Boundary Conditions, *SIAM J.Math. Anal.* **29** (1998) 1040–1065.
18. K.-H. Souleymane, V. Perrier, Effective construction of divergence-free wavelets on the square, *J. of Computational and Applied Math.* **240** (2013) 74–86.
19. K.-H. Souleymane, V. Perrier, Helmholtz-Hodge Decomposition on $[0, 1]^d$ by Divergence-free and Curl-free Wavelets, *Lecture Notes in Computer Science series* **6920** (2012), springer, 311–329.
20. R. Stevenson, Divergence-free wavelet bases on the hypercube, *Appl. Comput. Harmon. Anal.* (2010), doi:10.1016/j.acha.2010.01.007.
21. K. Urban, Wavelet Bases in H(*div*) and H(*curl*), *Math. Comput.* **70** (2000) 739–766.

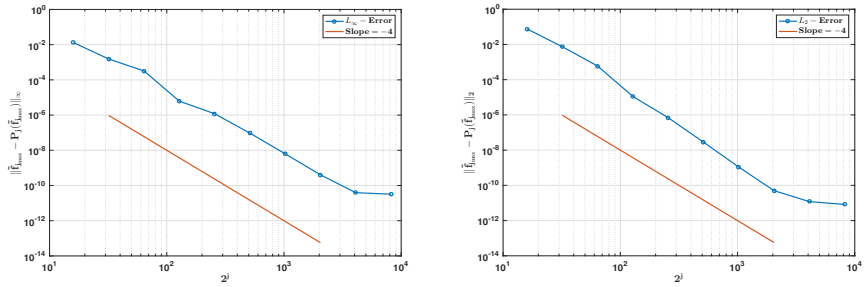

Fig. 15: Plot of the projection error $\|\tilde{f}_{j_{max}} - \mathcal{P}_j^1(\tilde{f}_{j_{max}})\|_\infty$ (left) and $\|\tilde{f}_{j_{max}} - \mathcal{P}_j^1(\tilde{f}_{j_{max}})\|_2$ (right) in loglog scale, where (φ^0, ψ^0) are Daubechies orthogonal generators with $r = 3$

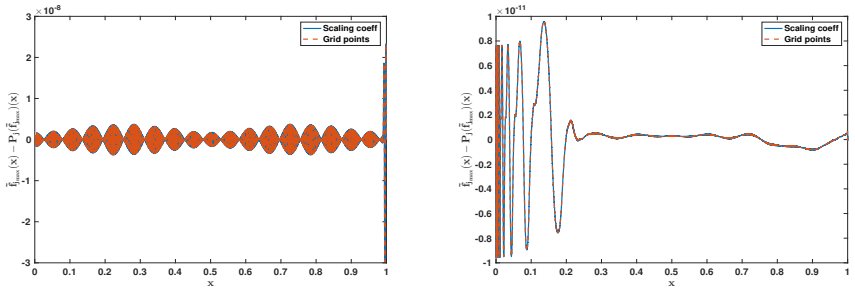

Fig. 16: Plot of the projection error $\tilde{f}_{j_{max}} - \mathcal{P}_j^1(\tilde{f}_{j_{max}})$ at grid points for $j_{max} = 16$ and $j = 9$ (left) and for $j = 13$ (right), where (φ^0, ψ^0) are Daubechies orthogonal generators with $r = 3$.

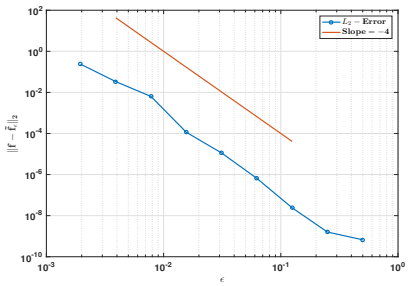

Fig. 17: Plot of the non linear approximation L_2-errror. Daubechies orthogonal generator with $r = 3$.

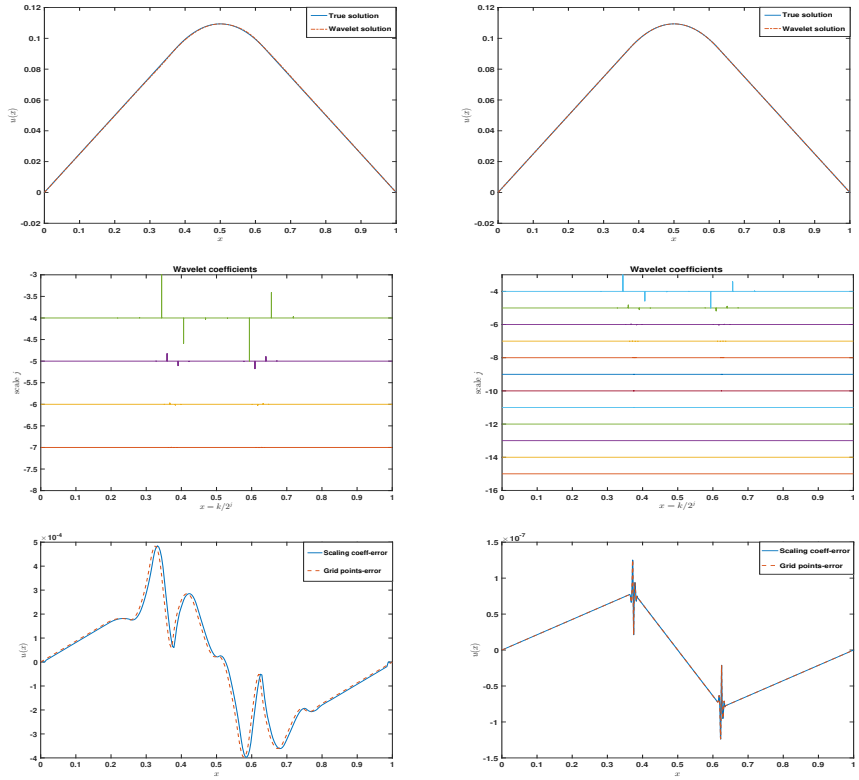

Fig. 18: From top to bottom, plot of the computed solution, its wavelet coefficients and the residual error (first column $j = 8$ and second column $j = 16$). Where (φ^0, ψ^0) are Daubechies orthogonal generators with $r = 3$.